Catal Lett (2008) 126:268–274
DOI 10.1007/s10562-008-9623-1

Effect of TiO_2–Al_2O_3 Sol–Gel Supports on the Superficial Ni and Mo Species in Oxidized and Sulfided NiMo/TiO_2–Al_2O_3 Catalysts: Influence on Dibenzothiophene Hydrodesulfurization

A. Guevara · A. Alvarez · M. Vrinat

Received: 30 May 2008 / Accepted: 18 August 2008 / Published online: 23 September 2008

Abstract The present work presents a comparative study of NiMo catalysts supported on sol–gel TiO_2–Al_2O_3 mixed oxides with 5 and 95 mol% content of Al_2O_3. The DRX and N_2 physisorption results showed that the sol–gel method allows preparation of TiO_2–Al_2O_3 mixed oxides possessing high superficial area and an amorphous TiO_2 structure. Results of ζ-potential showed that the net surface pH of the supports depends on their structure and composition. According to UV–Vis and Raman spectra obtained from the solids after impregnation, catalysts with high content of Al_2O_3 showed $Mo_7O_{24}^{2-}$ and $Mo_8O_{26}^{4-}$ species displaying Mo–O–Mo stretching vibration modes. On the other hand, catalysts with high content of TiO_2 showed $Mo_7O_{24}^{2-}$ and $Mo_8O_{26}^{4-}$ species with vibration modes corresponding to terminal Mo=O_t bonds. Therefore, it appears that impregnation of catalysts with a pH 9 solution allows a polymerization process of MoO_4^{2-} and $[Ni^{2+}4O^{2-}]$ solution species to $Mo_8O_{26}^{4-}$ and $Mo_7O_{24}^{2-}$ species with a close interaction with $[Ni^{2+}6O^{2-}]$ species. However, these species have low interaction with the support. Thus, composition of the support appears to be more important than net surface pH in order to obtain a better distribution of superficial Mo species. XPS results suggest a higher proportion of "NiMoS" phase on the TiO_2 rich support. The most active catalyst in the dibenzothiophene hydrodesulfurization was NiMo/TiO_2–Al_2O_3 with 5 mol% Al_2O_3. This suggests that $Mo_7O_{24}^{2-}$ and $Mo_8O_{26}^{4-}$ in combination with $[Ni^{2+}6O^{2-}]$ species produce a better Ni/(Ni + Mo) ratio and NiMoS phase.

Keywords TiO_2–Al_2O_3 sol–gel · Hydrodesulfurization · Raman · UV–Vis diffuse reflectance · ζ-Potential

1 Introduction

Commercial diesel fuel contains sulfur compounds such as 4,6-dimethyl-dibenzothiophene which are difficult to remove during hydrodesulfurization (HDS) due to their low reactivity resulting from steric hindrance caused by the methyl groups [1, 2]. In order to achieve complete elimination of these refractory sulfur compounds, new catalysts prepared over supports that allow maximum dispersion of "NiMoS" catalytic active sites are required. The relationship between structure and catalytic activity of HDS catalysts containing Co or Ni-promoted MoS_2 clusters supported on γ-Al_2O_3 has been reviewed by Topsøe et al. [3]. These authors have reported that: "The CoMoS phase was shown to be MoS_2-like structures with the promoter (Co or Ni) atoms located at the edges in fivefold coordinates sites at the edge planes of MoS_2 [3]". Furthermore, these authors state that "For the alumina-supported catalysts, the single slab structure (called type I Co–Mo–S) interact strongly with the support, probably via Mo–O–Al linkages located at the edges. For the multiple slab form (called type II CoMoS) these interactions are small [3]". Coulier et al. [6] report that Ti acts as a promoter over MoS_2 catalyst. However, the low TiO_2 surface of this catalyst limits its application as support for hydrodesulfurization reactions. Recently, Shimada et al. [7, 8] reported

A. Guevara (✉) · A. Alvarez
Centro de Investigaciones Químicas, Universidad Autónoma del Estado de Hidalgo, Carr. Pachuca-Tulancingo Km. 4.5, Ciudad Universitaria, C.P. 42184 Pachuca, Hidalgo, Mexico
e-mail: guevaraa@uaeh.edu.mx

M. Vrinat
Institut de Recherches sur la Catalyse et de l'Environnent de Lyon, CNRS, 2 Av. Albert Einstein, 69626 Villeurbanne Cedex, France

that MoS_2 clusters supported on TiO_2 (anatase) are edge-bonded multi-layer MoS_2 clusters which allow a better availability of active sites and overcome the steric hindrance of the sulfur compounds on the catalyst surface. Sakashita [9] proposed that precursors of the edge-bonded multi-layer MoS_2 clusters are formed during preparation of catalyst oxides. On the contrary, Van Veen and Hendriks [10] reported that TiO_2 does not really adsorb Mo species, but does allow formation of a superficial Mo precipitate. Therefore, more attention has been paid to applications of TiO_2–Al_2O_3 mixed oxides [11–16] as supports of hydrodesulphurization catalysts. To our knowledge, there are only a few studies about Ni–Mo/support interactions. The aim of this work was to improve our knowledge of molecular Ni–Mo–support interactions by studying two sol–gel TiO_2–Al_2O_3 supports and their effects on the superficial properties of molybdenum catalysts promoted with nickel.

2 Experimental

2.1 Catalysts Preparation

TiO_2–Al_2O_3 supports were prepared by the sol–gel method under a N_2 atmosphere. Alkoxide precursors, $Al(OC_3H_7)_3$ and $Ti(OC_3H_7)_4$, were dissolved in *i*-propanol (1 g isopropoxide/10 ml of isopropanol). The resulting solution was refluxed for 12 h at 353 K. The gel was obtained by hydrolysis of this material with the dropwise addition of a 0.01 M NH_4OH solution. The gel was then dried by evaporation at 373 K for 12 h and calcinated at 823 K (5 K/min) for 6 h. These solids with concentration of 5 or 95 mol% of Al_2O_3 will be referred to as: Ti95Al5 and Ti5Al95, respectively. The supports, crushed and sieved (100–150 mesh) were co-impregnated with an aqueous $(NH_4)_6MoO_76H_2O + Ni(NO_3)_2 \cdot 6H_2O$ solution in order to get a concentration of 12 wt% of MoO_3 and a Ni/(Ni + Mo) ratio = 0.3 using the incipient wetness impregnation technique. In order to have an impregnation solution with MoO_4^{2-} and $[Ni^{2+}4O^{2-}]$ species, the pH solution was adjusted to 9 by addition of a 0.01 M NH_4OH solution. These solids were kept at room temperature for 24 h and then dried at 383 K for 4 h.

2.2 Catalysts Characterization

Supports were characterized by N_2 physisorption, X-ray diffraction (XRD) and ζ-potential. N_2 physisorption was performed on an ASAP 2020 Micromeritics apparatus. The specific surface area was calculated by application of the Brunauer, Emmet, and Teller (BET) model. Previous to measurement, samples were treated at 573 K for 12 h under vacuum (30 μmmHg). XRD measurements were performed with a Phillips diffractometer using Cu Kα radiation ($\lambda = 1.5418$ Å) in a $15° < 2\theta < 80°$ (2°/min) range. ζ-Potential values were measured using a Malvern ZetaSizer 3000 apparatus; supports were prepared in a colloidal suspension of 0.05 g solid/L of aqueous solutions of KNO_3, 1×10^{-2} mol/L at 298 K. Catalysts in oxidized state were characterized by Raman and UV–Vis diffuse reflectance (UV–Vis DRS) spectroscopies. Raman spectra were recorded on a Perkin Elmer GX Raman FT-IR apparatus equipped with a Nd:YAG (1,064 nm) laser and an InGaAs detector. For each spectrum, an average of 10–50 scans were obtained with a laser power of 40–300 mW in the 1,500–100 cm^{-1} range, with a resolution of 2–4 cm^{-1}. UV–Vis DRS were recorded on a Perkin Elmer Lambda 40 spectrometer equipped with an integration sphere. As a reference for the UV–Vis DRS, we used the Spectralon SRS-99-010 (99% reflectance) tablet. In the recording of the reflectance data shown, the Kubelka–Munk ($F(R_\infty)$) function was applied:

$$F(R_\infty) = \frac{(1 - R_\infty)^2}{2R_\infty}, \quad (1)$$

in which R_∞ is the reflectance at infinite depth.

Catalysts were activated by sulfidation with a flow of 4 L/h of a 10 mol% H_2S/H_2 gas mixture at 673 K (5 K/min) during 4 h. Regarding Ti and Al% composition, the catalysts will be referred to as NiMoS/Ti95Al5 and NiMoS/Ti5Al95, respectively. Sulfided catalysts were characterized by X-ray photoelectron spectroscopy (XPS). XPS measurements were performed using an ESCALAB 200 R instrument equipped with an energy source of Al Kα, $E = 1{,}486.6$ eV.

2.3 Catalytic Tests

Dibenzothiophene (DBT) hydrodesulfuration (HDS) was used to test catalytic properties. Tests were carried out in a continuous flow trickled-bed micro-reactor with 0.05 g of catalyst at 573 K and 30 bar. The reactor was fed with a 1.2×10^{-4} L/h (STP) of a solution of 0.37 mol of DBT in *n*-hexadecane and a flow of 2.2 L/h of H_2 (STP). *n*-Dodecane was added to the liquid fed as an internal standard for gas chromatography, in the same amount as DBT. Liquid samples were analyzed by gas chromatography on a Perkin Elmer Auto System instrument equipped with a FID detector and a HP-Ultra 2 (30 m × 0.32 mm i.d.) column. Main reaction products were biphenyl and cyclohexylbenzene. Reaction rates were calculated considering a first order kinetic and a differential reactor as follows:

$$r_i = \frac{F_{i_0} x_i}{m_c} \quad (2)$$

where F_{i_0} is the feeding molar flow of DBT, m_c the weight of catalyst, and x_i is the DBT conversion.

$$x_{DBT} = \frac{C_{DBT_0} - C_{DBT}}{C_{DBT_0}} = \frac{\sum A_i}{\sum A_i + A_{DBT}} \quad (3)$$

where A_i is the peak area of i products in the chromatogram.

3 Results and Discussion

3.1 Structure and Specific Surface Area of Supports

XRD patterns of TiO_2–Al_2O_3 supports are shown in Fig. 1. Although peaks detected are weak their pattern corresponds to γ-Al_2O_3, JCPDS-290063 [17]. No peak corresponding to titanium oxide was detected. Due to the high concentration of TiO_2, this lack of peaks suggests that titanium oxide is amorphous. It should be pointed out the dependence of the Bragg peak width on particle size. Thus, as the average powder particle size decreases below 200 nm, the diffracted peaks increase their width and diminish their intensity [18]. Surface areas of samples are summarized in Table 1. BET surface area of mixed oxides increases with TiO_2 content. These results indicate that the sol–gel method is adequate to prepare TiO_2–Al_2O_3 mixed oxides with a high surface area and an amorphous TiO_2 structure, even after calcination at 823 K.

3.2 Effect of Al_2O_3 Content on the Net Surface pH of Solids: ζ-Potential

Figure 2 shows variation of ζ-potential as a function of the solution pH. Both solids gave similar curves, which indicate that the solids have a similar superficial net charge. The point at which $\zeta = 0$ is called the iso-electric point

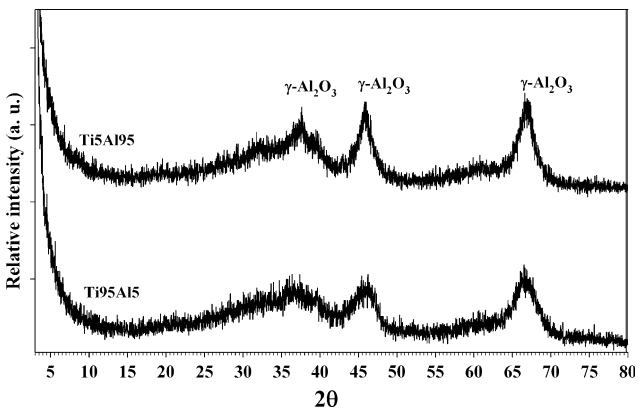

Fig. 1 X-ray diffraction patterns of TiO_2–Al_2O_3 oxides

Table 1 BET area and net surface pH of mixed TiO_2–Al_2O_3 oxides

Support	A_{BET} (m^2/g)	Net surface pH
Ti5Al95	280	7
Ti95Al5	363	8

(*i.e.p.*) and the fact that it is independent of the ionic strength of KNO_3 suggests that, in this case, the *i.e.p.* is the same as the point of zero charge (*p.z.c*). In short, the ζ-potential method relies on the assumption that if the solid is placed in a solution of the same pH as the *p.z.c.,* it will not cause a change in the pH of the solution. Therefore, it is possible to associate the *p.z.c.*, or *i.e.p.* to net surface pH of TiO_2–Al_2O_3 supports [19]. Parks [20] reported that net surface pH of γ-Al_2O_3 and TiO_2 (anatase) are 8.0 and 6.2, respectively. Table 1 shows that net surface pH of Ti95Al5 is 7 whereas that of Ti5Al95 is 8. These net surface pH values indicate that 5 mol% of TiO_2 did not modify the superficial net charge of γ-Al_2O_3. However, 5 mol% of γ-Al_2O_3 is enough to modify the structure and net surface pH of TiO_2.

3.3 Characterization of NiMo/TiO_2–Al_2O_3 Precursors

3.3.1 Raman Spectroscopy

NiMo impregnated catalysts not submitted to calcination have a high content of humidity. Therefore, hydrated species of superficial molybdenum oxides can be related to molybdenum oxides species in aqueous solutions [21, 22]. From this observation, Raman spectra of impregnation solutions as a pH function are given in Fig. 3. A Raman spectrum of impregnation solution at pH 9 shows bands at 897, 835, 312, and 300 cm^{-1} which correspond to isolated MoO_4^{2-} species of molybdenum ion with tetrahedral symmetry (Td). The impregnation solution with pH = 5.6 shows less intense bands at 945, 565, 350, and 230 cm^{-1} corresponding to

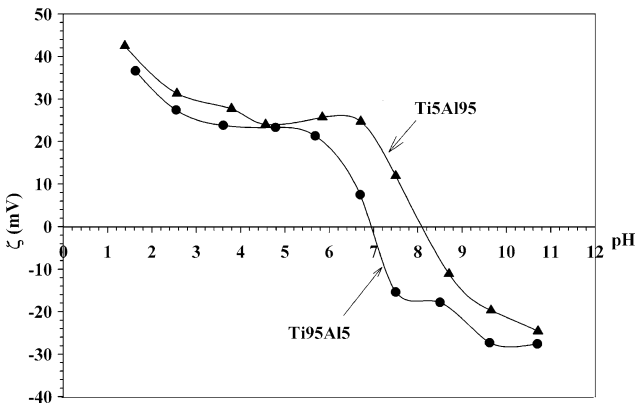

Fig. 2 ζ-Potential of colloidal TiO_2–Al_2O_3 as a function of pH solution, at 298 K

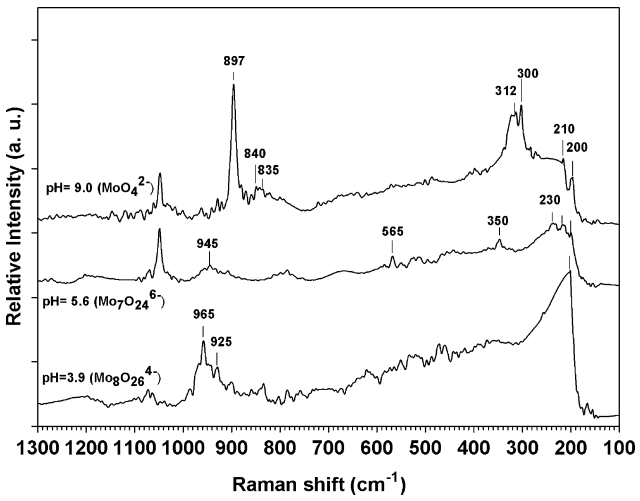

Fig. 3 Raman spectra of aqueous $(NH_4)_6Mo_7O_{24}4H_2O + Ni(NO_3)_2$ solution, $T = 298$ K

$Mo_7O_{24}^{6-}$ species with octahedral symmetry (Oh). The impregnation solution at pH = 3.9 shows bands at 965 and 200 cm^{-1} corresponding to $Mo_8O_{26}^{4-}$ species [23, 24]. Raman bands allow identification of vibration modes. Thus, the band around ~560 is assigned to Mo–O–Mo symmetric stretching and that at 210 cm^{-1} is assigned to a Mo–O–Mo deformation mode. Raman bands in regions between 890–1000 and 830–970 cm^{-1} are attributed to symmetric and asymmetric vibration modes of a terminal Mo=O_t bond, while bands around 310–370 cm^{-1} correspond to bending modes of a terminal Mo=O_t bond.

In order to elucidate the influence of net surface pH of TiO_2–Al_2O_3 supports on superficial molybdenum and nickel oxides species, TiO_2–Al_2O_3 supports were impregnated with a pH 9 solution, containing mainly tetrahedral molybdenum and nickel species. Raman spectra of NiMo/TiO_2–Al_2O_3 catalysts dried at 383 K are shown in Fig. 4.

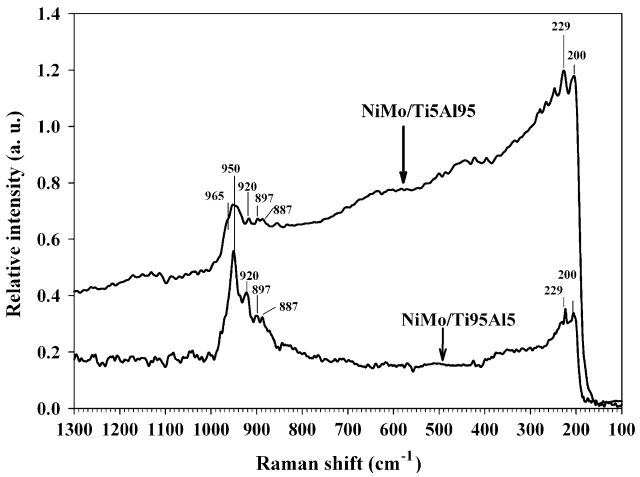

Fig. 4 Raman spectra of NiMo/TiO_2–Al_2O_3 catalysts as a function of support composition

Both catalysts show bands at 965, 950, 920, 897, 229, and 200 cm^{-1} which could be associated to $Mo_8O_{36}^{4-}$, $Mo_7O_{24}^{6-}$, and MoO_4^{2-} ions. These ions indicate a polymerization of Mo species. Thus, MoO_4^{2-} in solution polymerizes to $Mo_7O_{24}^{6-}$ and $Mo_8O_{26}^{4-}$ species on the support. This type of polymerization has been associated to net surface pH of support [23, 24]. However, support composition should also be taken into account. In the case of NiMo/Ti5Al95 solid, the band observed at 229 cm^{-1} is relatively more intense than that at 950 cm^{-1}, therefore, $Mo_7O_{24}^{6-}$ ions have Mo–O–Mo symmetric stretching and deformation modes. These vibration modes indicate that $Mo_7O_{24}^{6-}$ has a high Mo–O–support interaction with the Ti5Al95 support [25, 26]. On the case of the NiMo/Ti95Al5 catalyst, the 950 cm^{-1} band is relatively more intense that other bands, indicating a high quantity of $Mo_7O_{24}^{6-}$ ions with vibrational Mo=O_t bonds. Therefore, the small interaction between MoO_4^{2-} species and supports allows formation of superficial $Mo_8O_{36}^{4-}$ and $Mo_7O_{24}^{6-}$ ions on both supports.

3.4 Effect of Al_2O_3 Content on Superficial Structure of Nickel Oxide in NiMo/TiO_2–Al_2O_3 Precursors: UV–Vis Spectroscopy

Figure 5 shows UV–Vis absorbance spectra of impregnation solutions as a function of pH. Assignment of absorption bands in UV–Vis spectra of catalysts was carried out according to literature [27–30]. Bands at 393 and 376 nm are associated to $[Ni(H_2O)_6]^{2+}$; bands around 623 and 650 nm can be assigned to Ni^{2+} ions with tetrahedral coordination symmetry; bands about 710 and 736 nm can be assigned to Ni^{2+} ions with octahedral coordination symmetry. At pH 9, an intense absorption band at 623 nm

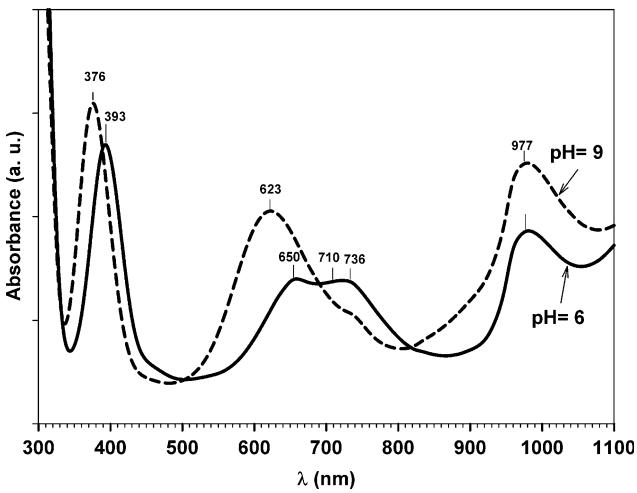

Fig. 5 UV–Vis absorption spectra of aqueous $(NH_4)_6Mo_7O_{24}4H_2O + Ni(NO_3)_2$ solutions, $T = 298$ K

is observed, suggesting that $[Ni^{2+}4O^{2-}]$ predominates in the impregnation solution. At pH 6, the intensity of absorption bands is similar for $[Ni^{2+}4O^{2-}]$ and $[Ni^{2+}8O^{2-}]$ ions, suggesting that at pH $\sim$ 6 both complexes can be found. A band about 977 nm is assigned to Ni^{2+} cation in distorted tetrahedral symmetry. Previous studies about nickel oxides supported on alumina and zeolite [29, 30] report that the coordination symmetry of Ni^{2+} ion depends on the degree of interaction between Ni^{2+} and support. Therefore, these bands could be shifted due to Ni–Mo–support interactions.

UV–Vis DRS of NiMo/TiO_2–Al_2O_3 catalysts are shown in Fig. 6. TiO_2–Al_2O_3 supports do not show bands in the 350–1,100 nm region. NiMo/Ti5Al95 oxide presents a triplet with bands at 650, 710, and 750 nm. In this case, the most intense band is that at 650 nm. This suggests that Al_2O_3 favors tetrahedral $[Ni^{2+}4O^{2-}]$ ions. It has previously been reported [3, 28, 29] that a tetrahedral symmetry of Ni^{2+} could be associated to a large Ni–support interaction. Then, during impregnation, the interaction between Ni and support is strong and then polymerization of MoO_4^{2-} to $Mo_7O_{24}^{6-}$ does not capture Ni^{2+} ions inside the polymer. On the other side, NiMo/Ti95Al5 shows that intensity of the 650 nm band is lower than those at 710 and 760 nm. This indicates that Ni^{2+} ions mainly have octahedral symmetry. We reported [31] that octahedral Ni^{2+} bands could be associated to Ni–Mo clusters with a close interaction. Therefore, in this case, interactions between Ni and Mo species are more important that those between Ni and support. Thus, during polymerization of MoO_4^{2-} to $Mo_7O_{24}^{6-}$, Ni^{2+} is closely attached to Mo. It should be noted that the 342 nm band indicates supported nickel hydroxide; whose formation is due to small interactions between Ni and support.

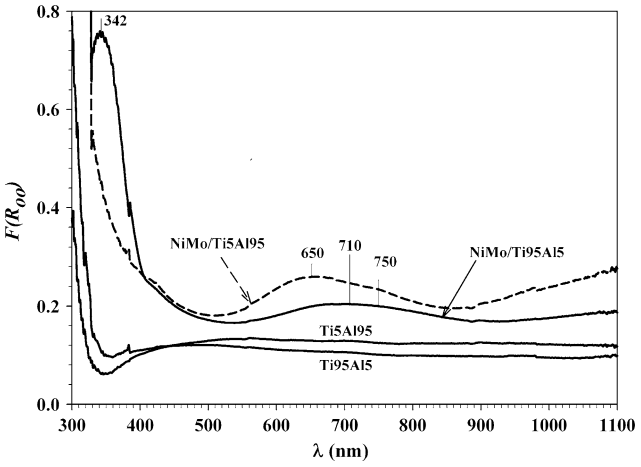

Fig. 6 UV–Vis RDS of NiMo/TiO_2–Al_2O_3 precursors as a function of support composition

3.5 Characterization of NiMo/TiO_2–Al_2O_3 Sulfides

3.5.1 X-ray Photoelectronic Spectroscopy

XPS results are reported in Table 2. The binding energies are referred to C 1s a 284.6 eV. Mo 3d decomposition spectra show existence of two Mo oxidation states: Mo^{4+} and Mo^{5+} corresponding to MoS_2 [32] and molybdenum oxysulfide species [33], respectively. The 93 mol% content of Mo^{4+} in the NiMoS/Ti95Al5 indicates a better sulfidation for this catalyst compared to the NiMoS/Ti5Al95 (76 mol% of Mo^{4+}). It is interesting to note a 0.2 eV difference of $Ni2p_{3/2}$ binding energy between the NiMoS/Ti95Al5 and NiMo/Ti5Al95 [33]. This suggests formation of "NiMoS" phase over the TiO_2 rich support. NiMoS/Ti95Al5 shows a relative surface Ti/Al ratio of 3.12, suggesting that TiO_2 has an amorphous structure as suggested by XRD results.

3.6 Hydrodesulphurization of Dibenzothiophene

Rates of transformation of DBT as a function of support composition were determined and the results are shown in Table 3. After 8 h, catalysts reach a pseudo-stationary state. In both cases, biphenyl and cyclohexylbenzene were observed as products of DBT transformation. The NiMoS/Ti95Al5 was the most active and most stable catalyst. This result suggests that $Mo_7O_{24}^{6-}$ species with terminal Mo=O bonds and Ni^{2+} ions with octahedral coordination $[Ni^{2+}6O^{2-}]$ are the best precursors of an active catalyst.

4 Discussion

Our results show that use of aluminum and titanium alkoxides allow preparation of TiO_2–Al_2O_3 supports having large surface areas by the sol–gel method. Therefore, such solids could be considered for preparation of hydrotreating catalysts.

Table 2 XPS analysis of sulfided NiMo/TiO_2–Al_2O_3 Catalysts

	Mo $3d_{3/2}$ Mo^{4+}	Mo $3d_{3/2}$ Mo^{5+}	Ni $2p_{3/2}$	Al 2p	Ti $2p_{3/2}$	C 1s	S 2p	Ni/(Ni + Mo) (mol)	Ti/Al (mol)
Ti95Al5	228.4 (93%)	230.1 (7%)	854.8	73.7	458.9	284.6	161.7	0.37	3.12
Ti5Al95	228.1 (76%)	229.4 (24%)	855.0	73.9	459.5	284.6	161.7	0.24	0.043

Table 3 Hydrodesulfurization of dibenzothiophene

Catalysts	r ($\times 10^{-8}$ mol/s g cat)	Biphenyl	CHB
NiMoS/Ti5Al95	11.5	60	40
NiMoS/Ti95Al5	17.4	70	30

$P = 30$ bar, $T = 573$ K

Net surface pH of TiO_2–Al_2O_3 mixed oxides was determined by ζ-potential. Results showed that for high TiO_2 content (Ti95Al5) the net surface pH was about 7. Whereas, a pH value of 8 was obtained in the case of high Al_2O_3 content (Ti5Al95). Apparently, the γ-Al_2O_3 (*i.e.p.* = 8) structure favors the basic character of these supports.

In order to understand how the support can control distribution and nature of molybdenum and nickel species on the surface of oxidized catalysts, solids were characterized by Raman and UV–Vis spectroscopies after impregnation and drying. It has been reported [23, 24] that distribution of superficial MoO_3, $Mo_8O_{26}^{4-}$, $Mo_7O_{24}^{6-}$, and MoO_4^{2-} species is controlled by net surface pH of support. If we consider this proposition, the net surface pH 7–8 of Ti95Al5 and Ti5Al95 supports would allow principally MoO_4^{2-} species. However, comparison of spectra given in Figs. 3 and 4 indicates the presence of polymeric molybdenum species, after impregnation with a solution at pH 9, on both solids. Such species correspond to superficial $Mo_7O_{24}^{6-}$ and $Mo_8O_{26}^{4-}$ ions. These results suggest that superficial Mo distribution is controlled by net surface pH and by interaction between Mo and support. During impregnation, the small interaction between MoO_4^{2-} and support allows formation of $Mo_7O_{24}^{6-}$ and $Mo_8O_{26}^{4-}$ ions.

Comparison of spectra given in Figs. 5 and 6 indicate the coexistence of $[Ni^{2+}4O^{2-}]$ and $[Ni^{2+}6O^{2-}]$ complexes. However, the $[Ni^{2+}4O^{2-}]$ band is more intense on the Ti5Al5 support than on Ti95Al5. This indicates that Ni–support interaction is more important on the case of Ti5Al95 support than that of Ti95Al5. Then, impregnation with a pH 9 solution allows a polymerization process of MoO_4^{2-} and $[Ni^{2+}4O^{2-}]$ solution species to $Mo_8O_{26}^{4-}$ and $Mo_7O_{24}^{6-}$ species with a close interaction with $[Ni^{2+}6O^{2-}]$ on the Ti95Al5 support.

It appears that $Mo_8O_{26}^{4-}$ and $Mo_7O_{24}^{6-}$ ions with terminal Mo=O bonds and Ni^{2+} ions with octahedral symmetry are best precursors for HDS catalysts. This is confirmed by XPS and dibenzothiophene hydrodesulfurization results which showed a higher Mo^{4+} concentration on NiMoS/Ti95Al5 than on NiMoS/Ti5Al95 catalysts. These results also show a better formation of NiMoS phase, leading to a higher activity in dibenzothiophene hydrodesulfurization.

5 Conclusions

The sol–gel method has been used for preparation of TiO_2–Al_2O_3 mixed oxides with 95 and 5 mol% of Al_2O_3. Impregnation with a pH 9 solution allowed concluding that net surface pH and support composition affect distribution of superficial molybdenum oxide. This Mo distribution is rather controlled by small interaction between Ni and Mo species and supports. Catalytic activities in dibenzothiophene hydrodesulfurization show that $Mo_8O_{26}^{4-}$ and $Mo_7O_{24}^{2-}$ ions closely interacting with $[Ni^{2+}6O^{2-}]$ ions are optimal for formation of a HDS active NiMoS phase.

Acknowledgment The authors thank Scientific Cooperation Program CONACYT(Mexico)–CNRS(France) for financial support.

References

1. Macaud M, Milenkovic A, Schulz E, Lemaire M, Vrinat M (2000) J Catal 193:255–263
2. Meille V, Schulz E, Vrinat M (1999) Appl Catal A: Gen 187:179–186
3. Topsøe H, Clasusen BS, Massot FE (1996) Hydrotreating catalysis: science and technology. Springer, Berlin
4. Topsøe H, Clausen BS, Topsøe N-Y, Zeuthen P (1990) Stud Surf Sci Catal 53:77
5. Hensen EJM, de Beer VJH, van Veen JAR, van Santen RA (2002) Catal Lett 84:59–67
6. Coulier L, van Veen JAR, Niemantsverdriet JW (2002) Catal Lett 79:149–155
7. Araki Y, Honna K, Shimada H (2002) J Catal 207:361–370
8. Shimada H (2003) Catal Today 86:17–29
9. Sakashita Y (2001) Surf Sci 489:45–58
10. Van Veen JAR, Hendriks PAJM (1986) Polyhedron 5:75–78
11. Ramirez J, Fuentes S, Diaz G, Vrinat M, Breysse M, Lacroix M (1989) Appl Catal 52:211–224
12. McVicker JB, Ziemiak JJ (1985) J Catal 95:473–481
13. Foger K, Anderson JR (1986) Appl Catal A: Gen 23:139–155
14. Stranick A, Houalla M, Hercules DM (1990) J Catal 125:214–226
15. Wei ZB, Xin Q, Guo XX (1992) Catal Lett 15:255–261
16. Ramirez J, Ruiz-Ramirez L, Cedeno L, Harle V, Vrinat M, Breysse M (1993) Appl Catal A: Gen 93:163–180
17. International Centre for Diffraction Data (1993) Mineral power diffraction file: JCPDS. Pennsylvania, USA
18. Rohrer GS (2004) Structure and bonding in crystalline materials. Academic Press, Cambridge, pp 123–125
19. Hunter RJ (1981) Zeta potential in colloid science: principles and applications. In: Ottewill RH, Rowell RL (eds) Colloid science series. Academic, London
20. Parks AG (1965) Chem Rev 65:177–195
21. Spevac PA, McIntyre NS (1993) J Phys Chem 97:11020–11030
22. Kim DS, Segawa K, Soeya T, Wachs IE (1992) J Catal 136:539–553
23. Hu H, Bare SR, Wachs IE (1995) J Phys Chem 99:10897–10910
24. Deo G, Wachs IE (1991) J Phys Chem 95:5889–5895
25. Kasztelan S, Payen E, Toulhoat H, Grimblot J, Bonnelle JP (1986) Polyhedron 5:157–167
26. Blanchard P, Lamonier C, Griboval A, Payen E (2007) Appl Catal A: Gen 322:33–45
27. Lever AB (1984) Inorganic electronic spectroscopy, 2nd edn. In: Studies in physical theoretical chemistry, vol 33. Elsevier, Amsterdam, pp 507–711

28. Jacono ML, Sachiavello M, Cimino A (1971) J Phys Chem 75:1044–1050
29. Iova F, Trutia A (2000) Opt Mater 13:455–458
30. Lepetit C, Che M (1996) J Phys Chem 100:3137–3143
31. Guevara-Lara A, Bacaud R, Vrinat M (2007) Appl Catal A: Gen 328:99–108
32. Li CP, Hercules DM (1984) J Phys Chem 88:456
33. Houssenbay S, Kasztelan S, Toulhoat H, Bonnelle JP, Grimblot J (1989) J Phys Chem 93:7176–7180